



This is a repository copy of *Numerical study on comparison of Navier-Stokes and Burgers equations*.

White Rose Research Online URL for this paper:
<http://eprints.whiterose.ac.uk/78706/>

Version: Accepted Version

Article:

Ohkitani, K. and Dowker, M. (2012) Numerical study on comparison of Navier-Stokes and Burgers equations. *Physics of Fluids*, 24 (5). 055113. ISSN 1070-6631

<https://doi.org/10.1063/1.4719787>

Reuse

Unless indicated otherwise, fulltext items are protected by copyright with all rights reserved. The copyright exception in section 29 of the Copyright, Designs and Patents Act 1988 allows the making of a single copy solely for the purpose of non-commercial research or private study within the limits of fair dealing. The publisher or other rights-holder may allow further reproduction and re-use of this version - refer to the White Rose Research Online record for this item. Where records identify the publisher as the copyright holder, users can verify any specific terms of use on the publisher's website.

Takedown

If you consider content in White Rose Research Online to be in breach of UK law, please notify us by emailing eprints@whiterose.ac.uk including the URL of the record and the reason for the withdrawal request.



eprints@whiterose.ac.uk
<https://eprints.whiterose.ac.uk/>

Numerical Study on Comparison of Navier-Stokes and Burgers Equations

Koji Ohkitani and Mark Dowker

*School of Mathematics and Statistics, University of Sheffield,
Hicks Building, Hounsfield Road, Sheffield S3 7RH, United Kingdom*

(Dated: May 21, 2012)

Abstract

We compare freely decaying evolution of the Navier-Stokes equations with that of the 3D Burgers equations with the same kinematic viscosity and the same *incompressible* initial data by using direct numerical simulations. The Burgers equations are well-known to be regular by a maximum principle [Kiselev and Ladyzenskaya (1957)] unlike the Navier-Stokes equations.

It is found in the Burgers equations that the potential part of velocity becomes large in comparison with the solenoidal part which decays more quickly. The probability distribution of the nonlocal term $-\mathbf{u} \cdot \nabla p$, which spoils the maximum principle, in the local energy budget is studied in detail. It is basically symmetric, i.e. it can be either positive or negative with fluctuations. Its joint probability density functions with $\frac{1}{2}|\mathbf{u}|^2$ and with $\frac{1}{2}|\boldsymbol{\omega}|^2$ are also found to be symmetric, fluctuating at the same times as the probability density function of $-\mathbf{u} \cdot \nabla p$.

A power-law relationship is found in the mathematical bound for enstrophy $\frac{dQ}{dt} + 2\nu P \propto (Q^a P^b)^\alpha$, where Q and P denote the enstrophy and the palinstrophy, respectively and the exponents a and b are determined by calculus inequalities. We propose to quantify nonlinearity depletion by the exponent α on this basis.

I. INTRODUCTION

The regularity of the 3D Navier-Stokes equations is a well-known open problem despite lots of progress made in recent years. The mathematical literature are undoubtedly too numerous to cite them all here and we only quote [1–11] and references cited therein. In the areas of physical and engineering sciences, the regularity is more or less taken for granted. Nevertheless, the problem itself is also regarded as important in physical areas because the regularity is controlled by enstrophy, a physically important quantity closely related with turbulence. Indeed there are publications in this spirit [12–18].

In mathematical fluid mechanics, proofs of global regularity are obtained in a rather sporadic fashion. It is well known that the incompressible 2D Euler equations are regular for all time. The proof is based on conservation of scalar vorticity, which is a special property of the equations and no other proofs are known which do not depend on it.

As a related but simpler system, the 3D Burgers equations are known to possess globally regular solutions [19, 20]. In this case, because the nonlocal pressure term is absent, the maximum principle is valid and we conclude that the velocity is bounded at any time, if it is so initially. On the other hand, for the 3D Navier-Stokes equations, the possible formation of finite time singularities has not been ruled out, where a singularity means unbounded velocity. Nonetheless, the solutions of the Burgers equations are more singular than those of the Navier-Stokes equations in the sense that the width of shock waves $\propto \nu$ is thinner than the Kolmogorov dissipative scale $\propto \nu^{3/4}$ in Navier-Stokes turbulence. Furthermore the inviscid Burgers equations are known to have solutions that blow up in finite time, whereas for the Euler equations this is not known. For the Burgers equations, see also [21–24]. Thus it makes sense to give a more detailed comparison of these equations.

The purpose of this paper is (i) to compare these two equations in some details by numerical experiments and (ii) to characterize the notorious nonlocal effects in the Navier-Stokes equations by observing how the maximum principle actually breaks down. A comparison of PDFs (probability density functions) of the velocity with those of a passive scalar are also made. In Section II, mathematical formulation is given with a summary of known properties of these equations. In Section III, we compare numerically the Navier-Stokes with Burgers equations in detail. In Section IV, dynamics of a passive scalar is studied, centering on how its behavior is affected by a maximum principle. Performance of the enstrophy bounds are

assessed, including the quasi-4D Navier-Stokes equations. Section V is devoted to summary and discussion. All the numerical experiments concerned in this paper are those of freely decaying simulations.

II. MATHEMATICAL FORMULATION

We consider the incompressible 3D Navier-Stokes equations under periodic boundary conditions. With standard notations they read

$$\frac{\partial \mathbf{u}}{\partial t} + (\mathbf{u} \cdot \nabla) \mathbf{u} = -\nabla p + \nu \Delta \mathbf{u}, \quad (1)$$

$$\nabla \cdot \mathbf{u} = 0, \quad (2)$$

together with a smooth initial condition

$$\mathbf{u}(\mathbf{x}, t = 0) = \mathbf{u}_0(\mathbf{x}). \quad (3)$$

We can rewrite them equivalently as

$$\begin{aligned} \frac{\partial \mathbf{u}}{\partial t} &= \mathbf{u} \times \boldsymbol{\omega} - \nabla \left(p + \frac{|\mathbf{u}|^2}{2} \right) + \nu \Delta \mathbf{u} \\ &= \mathbf{P}(\mathbf{u} \times \boldsymbol{\omega}) + \nu \Delta \mathbf{u}, \end{aligned} \quad (4)$$

where \mathbf{P} denotes a solenoidal projection.

We also consider the 3D Burgers equations

$$\frac{\partial \mathbf{v}}{\partial t} + (\mathbf{v} \cdot \nabla) \mathbf{v} = \nu \Delta \mathbf{v}, \quad (5)$$

which are valid in any d -dimensions ($d = 1, 2, 3, \dots$). Because the velocity \mathbf{v} is not incompressible in general $\nabla \cdot \mathbf{v} \neq 0$, the energy budget equation takes the form

$$\frac{d}{dt} \int \frac{|\mathbf{v}|^2}{2} \mathbf{d}\mathbf{x} + \int (\mathbf{v} \cdot \nabla) \frac{|\mathbf{v}|^2}{2} \mathbf{d}\mathbf{x} = -\nu \int |\nabla \mathbf{v}|^2 \mathbf{d}\mathbf{x}. \quad (6)$$

Unlike the Navier-Stokes equations, the second term on the left does not vanish because of the compressible character of the velocity when $d \geq 2$. That is, we have no energy inequality for $d \geq 2$. However, for the 3D Burgers equations a maximum principle of the form

$$\max_{\mathbf{x}} |\mathbf{v}(\mathbf{x}, t)| \leq \max_{\mathbf{x}} |\mathbf{v}(\mathbf{x}, 0)|$$

is valid, which guarantees global-in-time regularity [20]. See the Appendix A for first integrals in the inviscid case.

It is a bit ironic that global regularity is known for the Burgers equations because of the maximum principle, even though we cannot establish the existence of weak solutions by the method of energy inequality as in the case of the Navier-Stokes equations.

A sketch of the argument is as follows. The local energy budget for the Navier-Stokes equations reads

$$\begin{aligned} \left(\frac{\partial}{\partial t} + \mathbf{u} \cdot \nabla \right) \frac{|\mathbf{u}|^2}{2} &= -\mathbf{u} \cdot \nabla p + \nu \mathbf{u} \Delta \mathbf{u} \\ &= -\mathbf{u} \cdot \nabla p - \nu |\nabla \mathbf{u}|^2 + \nu \Delta \frac{|\mathbf{u}|^2}{2} \end{aligned}$$

It follows that, because the advection term is zero at local maxima of the energy density,

$$\frac{\partial}{\partial t} \frac{|\mathbf{u}|^2}{2} \leq -\mathbf{u} \cdot \nabla p + \nu \Delta \frac{|\mathbf{u}|^2}{2}. \quad (7)$$

Because of the pressure term, we do not have a maximum principle unlike the case of the Burgers equations, e.g. [25]. For the Navier-Stokes equations, global regularity is obtained only for sufficiently large viscosity, or for sufficiently small initial data. With arbitrary viscosity and initial data, only the local existence of classical solutions has been established.

We consider the Helmholtz-Hodge decomposition for the Burgers equations taking a constant term to be zero,

$$\mathbf{v} = \mathbf{v}^\perp + \mathbf{v}^\parallel, \quad (8)$$

where \mathbf{v}^\perp and \mathbf{v}^\parallel denote solenoidal and compressible components, respectively and

$$\nabla \cdot \mathbf{v}^\perp = 0, \quad \nabla \times \mathbf{v}^\parallel = 0. \quad (9)$$

The solenoidal component can be written as

$$\mathbf{v}^\perp = \nabla \times \mathbf{A} \quad \text{with} \quad \nabla \cdot \mathbf{A} = 0, \quad (10)$$

whereas the potential component as

$$\mathbf{v}^\parallel = \nabla \phi. \quad (11)$$

Only when $\mathbf{v}^\perp = 0$ can the Cole-Hopf transform

$$\mathbf{v} = -2\nu \nabla \log \psi$$

be applied to yield [26]

$$\mathbf{v}_t + \mathbf{v} \cdot \nabla \mathbf{v} - \nu \Delta \mathbf{v} = -2\nu \nabla \left(\frac{\psi_t - \nu \Delta \psi}{\psi} \right), \quad (12)$$

which reduces (5) to a heat diffusion equation. Needless to mention, global regularity is obvious in this case.

The governing equations for each component can be derived as follows. By a well-known identity $\nabla \frac{|\mathbf{v}|^2}{2} = \mathbf{v} \cdot \nabla \mathbf{v} + \mathbf{v} \times \boldsymbol{\omega}$, we recast (5) as

$$\frac{\partial \mathbf{v}}{\partial t} = \mathbf{v} \times \boldsymbol{\omega} - \nabla \frac{|\mathbf{v}|^2}{2} + \nu \Delta \mathbf{v}.$$

Writing $\mathbf{v} \times \boldsymbol{\omega} = \mathbf{P}(\mathbf{v} \times \boldsymbol{\omega}) + (\mathbf{I} - \mathbf{P})(\mathbf{v} \times \boldsymbol{\omega}) = \nabla \times \mathbf{B} + \nabla \psi$ with $\mathbf{B} \equiv -\Delta^{-1} \nabla \times (\mathbf{v} \times \boldsymbol{\omega})$ and $\psi = \Delta^{-1} \nabla \cdot (\mathbf{v} \times \boldsymbol{\omega})$, we find

$$\begin{cases} \frac{\partial \mathbf{v}^\perp}{\partial t} = \mathbf{P}(\mathbf{v}^\perp \times \boldsymbol{\omega}) + \nu \Delta \mathbf{v}^\perp + \mathbf{P}(\mathbf{v}^\parallel \times \boldsymbol{\omega}), \\ \frac{\partial \mathbf{v}^\parallel}{\partial t} = -\nabla \frac{|\mathbf{v}|^2}{2} + (\mathbf{I} - \mathbf{P})(\mathbf{v} \times \boldsymbol{\omega}) + \nu \Delta \mathbf{v}^\parallel, \end{cases} \quad (13)$$

where \mathbf{I} is the identity matrix.

Note that the first equation of (13) reduces to the 3D Navier-Stokes equations *if* we ignore the final term of the right-hand-side of it. If we use the impulse formalism we may choose a gauge where the solenoidal component solves the Navier-Stokes equations and the potential component the Burgers equations (see Appendix B).

For more quantitative comparison we define some norms. The total energy may also be split in two parts:

$$\frac{1}{2} \langle |\mathbf{v}|^2 \rangle = \frac{1}{2} \langle |\mathbf{v}^\perp|^2 \rangle + \frac{1}{2} \langle |\mathbf{v}^\parallel|^2 \rangle, \quad (14)$$

which may be written $e(t) = e^\perp(t) + e^\parallel(t)$. Here the brackets denote a spatial average $\langle \rangle = \frac{1}{(2\pi)^3} \int d\mathbf{x}$. We also have

$$\frac{1}{2} \langle |\nabla \mathbf{v}|^2 \rangle = \frac{1}{2} \langle |\nabla \mathbf{v}^\perp|^2 \rangle + \frac{1}{2} \langle |\nabla \mathbf{v}^\parallel|^2 \rangle, \quad (15)$$

which can be written $q(t) = q^\perp(t) + q^\parallel(t)$.

An overall comparison between the Navier-Stokes equations and the Burgers equations is summarized in Table I. Some, but not all, of the features listed above suggest that the Burgers equations are more singular than the Navier-Stokes equations. It makes sense to take a closer look at the comparison in order to better understand the role played by the pressure term associated with incompressibility in maintaining the regularity.

TABLE I. Navier-Stokes and Burgers equations (for $\nu \ll 1$).

In each category, features emphasized in bold represent more singular nature than the other.

	Navier-Stokes	Burgers
energy inequality	Yes	No ($n \geq 2$)
global weak solutions	Yes	No
energy spectrum $E(k)$	$k^{-5/3}$	k^{-2}
smallest scale	$\nu^{3/4}$	ν
maximum principle	No	Yes
global strong solutions	Unknown	Known
blowup of ideal cases	Unknown	Known

III. COMPARATIVE EXPERIMENTS TO THE BURGERS EQUATIONS

For this purpose we set up the following experiment: *Assume that we solve the 3D Navier-Stokes equations and the 3D Burgers equations starting from identical incompressible initial data and with the same viscosity. What will happen to the two components \mathbf{v}^\perp and \mathbf{v}^\parallel in the Helmholtz decomposition of the Burgers solution?* We will consider more specific questions below.

Direct numerical simulations of the Navier-Stokes equations are done under periodic boundary conditions in double-precision arithmetic, using a standard Fourier pseudo-spectral method. The time-marching is done by the fourth-order Runge-Kutta method. Typically we use 256^3 grid points with aliasing errors removed by the so-called 2/3-rule.

We consider for the most part Navier-Stokes flows starting from random initial conditions. The initial conditions are generated to have the energy spectrum

$$E(k) = ck^2 \exp(-k^2), \quad (16)$$

where the phases of Fourier components are randomized by pseudo-random numbers and the prefactor c is determined to give unit enstrophy. Here we define the energy spectrum by

$$E(k) = \frac{1}{2} \sum_{k \leq |\mathbf{k}| < k+1} |\mathbf{u}(\mathbf{k})|^2, \quad (17)$$

where $\mathbf{u}(\mathbf{k})$ is the Fourier coefficient of the velocity. The values of kinematic viscosity used are $\nu = 0.005$ and $\nu = 0.01$. We mainly discuss the case with $\nu = 0.005$ (used in all the

figures) and $\nu = 0.01$ is used to check numerical accuracy. The typical time increment is $\Delta t = 2 \times 10^{-3}$.

We consider freely-decaying flows only, mostly those developing from random initial conditions and also the Taylor-Green initial condition at the end of this paper. We consider the decomposition $\mathbf{v} = \mathbf{v}^\perp + \mathbf{v}^\parallel$ for the solution of the Burgers equation, assuming initially that $\mathbf{v}^\parallel(0) = 0$ (due to the incompressible initial data), and feed the Navier-Stokes equations the same initial data $\mathbf{u}(0) = \mathbf{v}^\parallel(0)$. We begin confirming that our numerical experiments have some standard properties known for these flows.

A. Energy and enstrophy

We study what happens to the decomposition of the Burgers equations. In Fig.1a, we show how each component of the energy evolves in the Burgers equations together with the energy in the Navier-Stokes equations. For the Burgers equations, the incompressible component $e^\perp(t)$ decays rapidly while the compressible part $e^\parallel(t)$ grows rapidly from zero, reaching a maximum just before $t = 2$. Both components keep decaying and become comparable later. For the Navier-Stokes equations, the decay of energy takes place but more slowly than the sum of the two components of the Burgers equations. In Fig.1b, we show a similar comparison in terms of the enstrophy. The compressible part rapidly increases from zero to attain a maximum around $t = 2$, which is as twice as large as the peak value of the incompressible part. The peak value of the total enstrophy of the Burgers equations is larger than that of the Navier-Stokes equations by a factor of 3 and a mild maximum is attained for the Navier-Stokes equations later around $t = 6$. These results are consistent with a view that the Burgers equations are more singular than the Navier-Stokes equations.

B. Energy spectra

Now we examine the difference by studying the energy spectra. In Fig.2, we show each component of the Fourier energy spectra

$$E(k) = E^\perp(k) + E^\parallel(k) \tag{18}$$

for the Burgers equations together with that of the Navier-Stokes equations. They are taken at the same time $t = 5$. For the Navier-Stokes equations the higher wave number part

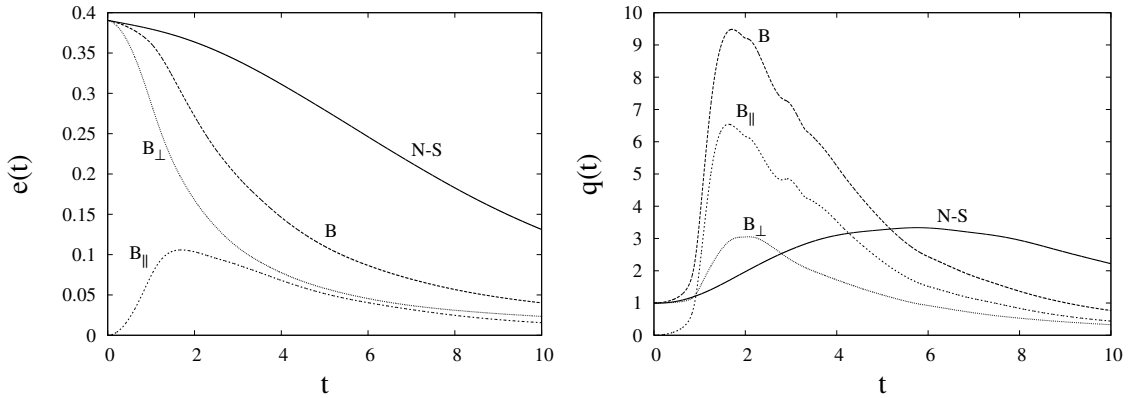


FIG. 1. Comparison of norms for the Navier-Stokes and Burgers equations: (a) the energy (left) and (b) the enstrophy (right). Here N-S stands for the Navier-Stokes equations, B for the Burgers equations, with B_{\perp} and B_{\parallel} representing the solenoidal and potential components of the Burgers equations respectively.

decays rapidly, while the Burgers equations have much more excitations in that range, which is marginally resolved. In the lower wave number range, we observe power-law behaviors close to k^{-2} in both $E^{\parallel}(k)$ and $E^{\perp}(k)$. For the Navier-Stokes equations, it is not clear if the flow displays $k^{-5/3}$ or not, because the viscosity $\nu = 0.005$ is not sufficiently small. Note that using the Navier-Stokes equations at a smaller value of viscosity and with a forcing term we may generate a power-law range consistent with $E(k) \propto k^{-5/3}$ (not shown). Actually, even at the current spatial resolution of 256^3 we can choose a smaller $\nu = 0.0025$ for the Navier-Stokes equations, but not for the Burgers equations because of truncation errors. Judging from the excitations at higher wavenumbers we observe that the Burgers equations are far more singular than the Navier-Stokes equations.

A few remarks regarding numerical accuracy for the computations are in order. We fit the energy spectrum as $E(k) = A(t)k^n(t) \exp(-\mu(t)k)$, where $A(t)$, $n(t)$ and $\mu(t)$ are determined by least-squares method. At $t = 2$, which is the least-resolved instant of time, the flow is somewhat under-resolved with $\mu(t = 2) = 2.25 \times 10^{-2} < \frac{2\pi}{N} = 2.45 \times 10^{-2}$ (mesh size) with $N = 256$. The flow is found to be better resolved at other times. We have conducted the same computation with 512^3 grid points to double-check that the evolution of the enstrophy in each component is independent of spatial resolutions (figure omitted). We have also confirmed that the dominance of the potential part over the the solenoidal part is seen in a well-resolved computation with $\nu = 0.01$. We conclude that the properties of the Burgers

equations obtained here are genuine, not numerical artifacts.

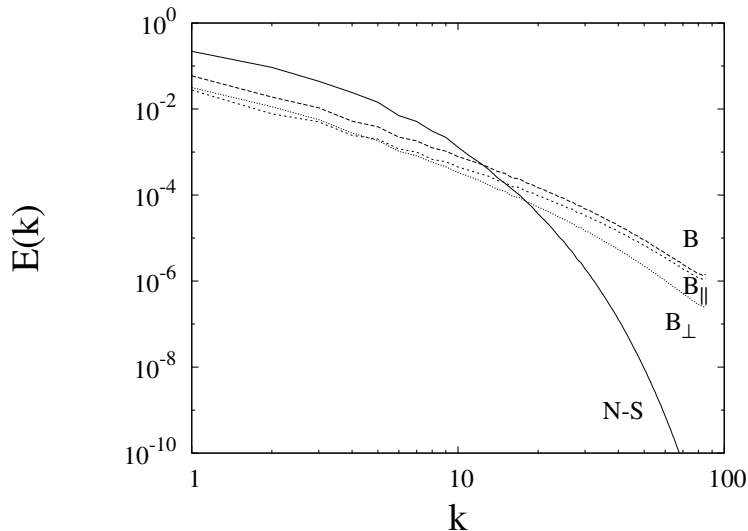


FIG. 2. Energy spectra $E(k)$ of the Navier-Stokes equations at $t = 5$ (solid), with corresponding $E(k)$ (dashed), $E(k)^\perp$ (short-dashed) and $E(k)^\parallel$ (dotted) for the Burgers equations at the same time. Symbols have the same meaning as in Fig.1.

C. Probability density function (PDF) of velocity

Now we consider how the absence of a maximum principle affects the dynamics of Navier-Stokes equations. It is well-known that the one-point PDF of a velocity component is close to a Gaussian distribution for Navier-Stokes turbulence. Fig.3a shows the time evolution of the PDF of the velocity, which is normalized to have unit variance. As time goes on, the tail parts spread toward larger amplitudes, getting closer to the normal Gaussian distribution. In contrast, for the Burgers equations the PDF behaves differently. That is, their wings remain restricted close to the initial profile (Fig.3b). This can be explained because the maximum principle precludes excitations at large amplitudes. Similar observations were made, for example, in [27] in a different context. We note that the PDFs of the velocity gradients distinguish the two equations more clearly; the Burgers equations are more intermittent than those of the Navier-Stokes equations (not shown here). We only consider the PDFs of velocity gradients because we are interested in the presence or absence of the maximum principle.

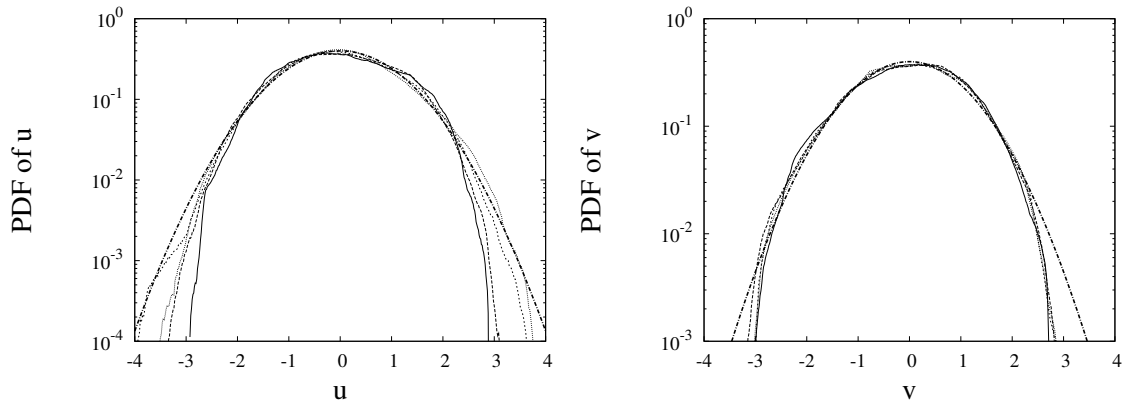


FIG. 3. PDFs of velocity field for a) the Navier-Stokes (left) and b) the Burgers (right) equations. Both are normalized to have unit variance: Plotted at $t = 2$ (solid), 5 (dashed), 8 (short-dashed) and 10 (dotted). The thicker dot-dashed lines denote the standard normal distribution $N(0, 1)$.

D. Nonlocal Term $-(\mathbf{u} \cdot \nabla)p$

It is this term which is responsible for the breakdown of the maximum principle for the Navier-Stokes equations. Therefore it makes sense to study the behaviors of the quantity in some detail. First, we show the PDF of $-(\mathbf{u} \cdot \nabla)p$ in Fig.4. We see that it is basically symmetric, that is, no preference is observed for positive or negative values. However, if we examine $-(\mathbf{u} \cdot \nabla)p$ at several different times in more detail, we see some fluctuations from time to time, occasionally making it skewed positively, e.g. at $t = 4$ (this point is to be examined below).

We study a possible correlation of these fluctuations with large energy or enstrophy, both of which are related with extreme events in Navier-Stokes equations. Shown in Fig.5a is a joint PDF between $-(\mathbf{u} \cdot \nabla)p$ and the local energy density $\frac{1}{2}|\mathbf{u}|^2$. There is no systematic trend of the sign of $-(\mathbf{u} \cdot \nabla)p$ correlated with large or small energy density. In fact, average of the local energy or enstrophy density, conditioned on the sign of $-(\mathbf{u} \cdot \nabla)p$ is 1:1 to within relative error of 1 %. A similar joint PDF with the local enstrophy density $\frac{1}{2}|\boldsymbol{\omega}|^2$ is given in Fig.5b. Again, there is no overall trend to be correlated with large or small enstrophy density, although a small negative fluctuation is seen for small values of $|\boldsymbol{\omega}|^2$ at $t = 4$. We have analyzed the data at other times and the slight fluctuations occur rarely and do not seem to follow any particular pattern. We conclude that the term $-(\mathbf{u} \cdot \nabla)p$ neither contributes to the formation of a singularity, nor to avoid it; it simply makes the maximum principle invalid.

In Fig.6a we plot the time evolution $|\mathbf{u}|_{\max}^2$, which sometimes exceeds its initial value. In Fig.6b we plot the skewness of $-(\mathbf{u} \cdot \nabla)p$. It should be noted that local maxima of $|\mathbf{u}|_{\max}^2$ at $t \approx 2, 4, 6$ are just preceded by those of the skewness factor. This means that fluctuations of the skewness factor correlate with local increase (or decrease) of the energy. If $-(\mathbf{u} \cdot \nabla)p$ is positively skewed instantaneously, it pumps up the energy at that time, as this term represents the inviscid contribution of the Lagrangian time derivative of local energy density.

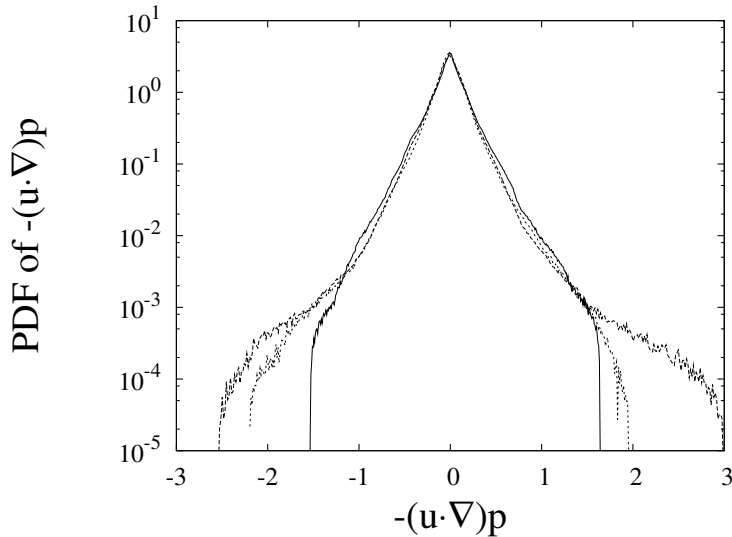


FIG. 4. The PDF of $-(\mathbf{u} \cdot \nabla)p$ at $t = 2$ (solid), $t = 4$ (dashed) and $t = 5$ (dotted), for the Navier-Stokes equations. Skewness correlates with the local maxima mentioned above and shown in Fig.6b. The quantity $-(\mathbf{u} \cdot \nabla)p$ is not normalized.

IV. PASSIVE SCALAR AS QUASI-4D NAVIER-STOKES FLOW

A. Passive scalar

We will consider a passive scalar field $\theta(\mathbf{x}, t)$ subject to the velocity in this section. The motivation is two-fold, 1) because differences between the Navier-Stokes and Burgers equations stem from the nonlocal pressure term, it makes sense to take a detailed look at the effect of nonlocality, and 2) to quantify numerically, in several spatial dimensions, the performance of the enstrophy bounds available mathematically. It should be kept in mind

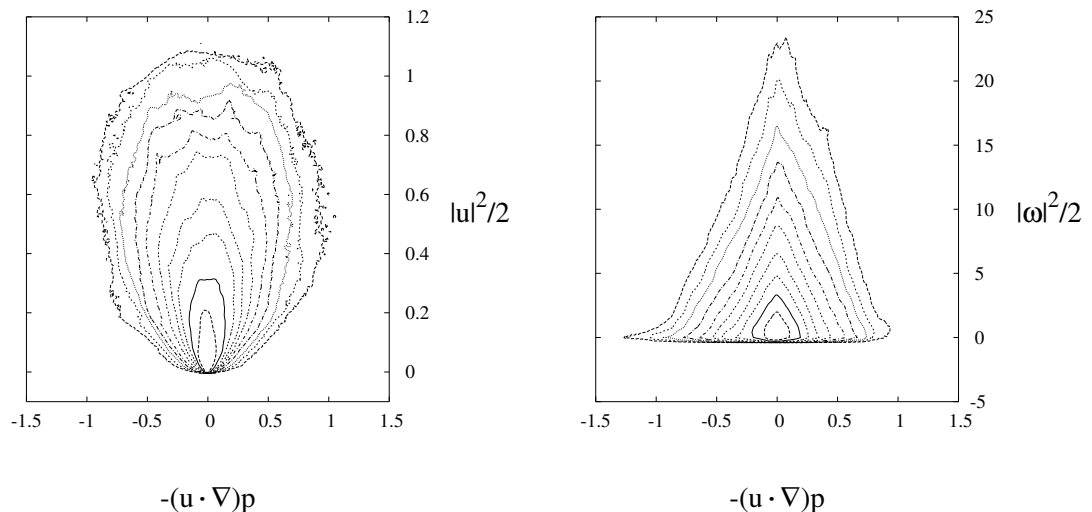


FIG. 5. Joint PDFs: (a) $-(\mathbf{u} \cdot \nabla)p$ and $\frac{1}{2}|\mathbf{u}|^2$ (left) and (b) $-(\mathbf{u} \cdot \nabla)p$ and $\frac{1}{2}|\boldsymbol{\omega}|^2$ (right) for the Navier-Stokes equations. The quantities are not normalized. Contour levels are set at $a(t)/2^n$, for $n = 0, 1, 2, \dots, 10$, where $a(t)$ is the maximum value of the PDF at the time instant (in this case $t = 4$).

that the pressure has both nonlocal and nonlinear characters, as is clear from its definition

$$p = -\Delta^{-1} \left(\frac{\partial u_i}{\partial x_j} \frac{\partial u_j}{\partial x_i} \right).$$

The equation for the passive scalar is given by

$$\frac{\partial \theta}{\partial t} + (\mathbf{u} \cdot \nabla)\theta = \nu \Delta \theta, \quad (19)$$

where θ is a passive scalar, \mathbf{u} is the solution of the 3D Navier-Stokes equations.

We take the diffusivity at the same value as the viscosity (unit Prandtl number) to make the comparison as parallel as possible. We initialize a passive scalar by $\theta(\mathbf{x}, 0) = u_1(\mathbf{x}, 0)$. Therefore any differences that may arise in the subsequent evolution between $u_1(\mathbf{x}, t)$ and $\theta(\mathbf{x}, t)$ for $t > 0$ should be attributed to the pressure gradient term [28]. In particular, by tracing the subsequent deviation we may monitor how the maximum principle breaks down for a component of velocity.

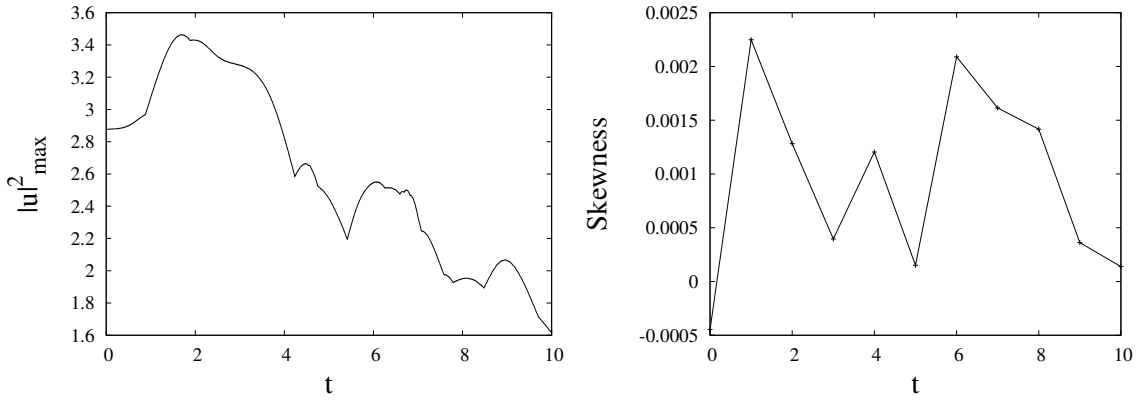


FIG. 6. Time evolution of (a) $\max |\mathbf{u}|^2$ (left) and (b) the skewness factor of $-(\mathbf{u} \cdot \nabla)p$ (right) for the Navier-Stokes equations.

In Fig.7, we compare evolution of the enstrophy $q(t)$ with the spatial average of the square of passive scalar gradient

$$q_\theta(t) = \frac{1}{2} \langle |\nabla \theta|^2 \rangle. \quad (20)$$

We note that $q_\theta(t)$ attains a maximum around $t = 3$ earlier than that of the enstrophy $q(t)$ at $t = 7$. Peak values are comparable. In Fig.8, we show energy spectrum $E(k)$ and passive scalar spectrum $E_\theta(k)$ at several different times.

$$E_\theta(k) = \frac{1}{2} \sum_{k \leq |\mathbf{k}| < k+1} |\boldsymbol{\theta}(\mathbf{k})|^2. \quad (21)$$

We observe that the slope of $E_\theta(k)$ is shallower than that of $E(k)$.

In order to study the difference in behavior of θ^2 and u_1^2 , we show in Fig.9 the time evolution of their maximum values. It should be noted that u_1^2 increases in the early stage in contrast to a monotonic decay of θ^2 , the latter behavior of course comes from the maximum principle. In Fig.10 we also show the time evolution of $\langle (u_1 - \theta)^2 \rangle$. Because of the initialization of θ , this is 0 at $t = 0$, and then grows in time because of the non-local effects. It attains a maximum around $t = 4$, which is between the times of maxima in $q(t)$ and $q_\theta(t)$. This suggests the nonlocal pressure term is intimately connected with the stretching of the vorticity and of the passive scalar gradient.

In Fig.11 we show iso-surface plots of $(u_1 - \theta)^2$, together with those of enstrophy. The large deviations and high enstrophy are correlated not only temporally but spatially. This indicates that the maximum principle breaks down in the vicinity of near-singular structure associated with large enstrophy. See also [27, 29].

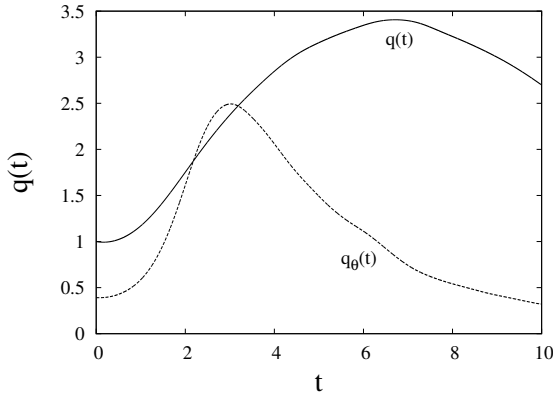


FIG. 7. Time evolution of $q(t)$ and $q_\theta(t)$ for the Navier-Stokes and passive scalar equations at $t = 5, 8$ and 10 .

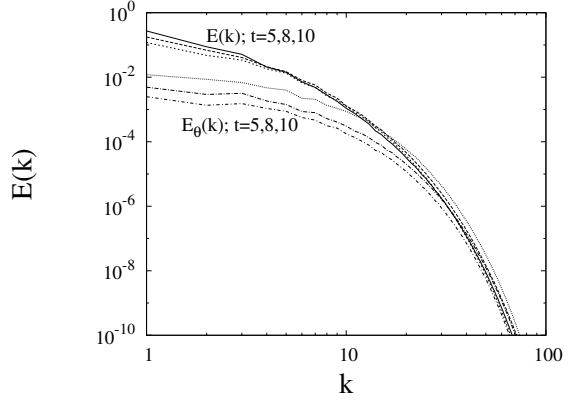


FIG. 8. Time evolution of energy spectra $E(k)$ and $E_\theta(k)$ of the Navier-Stokes and passive scalar equations at $t = 5, 8$ and 10 , respectively (in descending order from the top line).

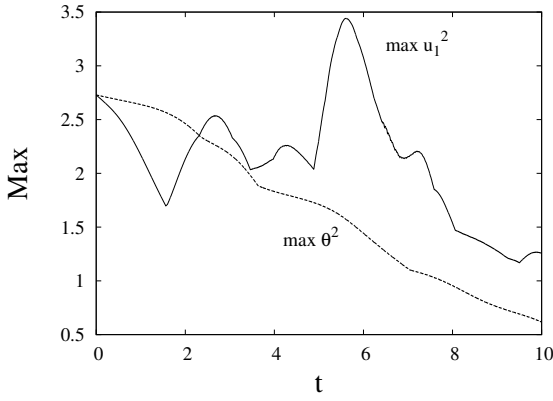


FIG. 9. Time evolution of $\max u_1^2$ and $\max \theta^2$ for the Navier-Stokes and passive scalar equations.

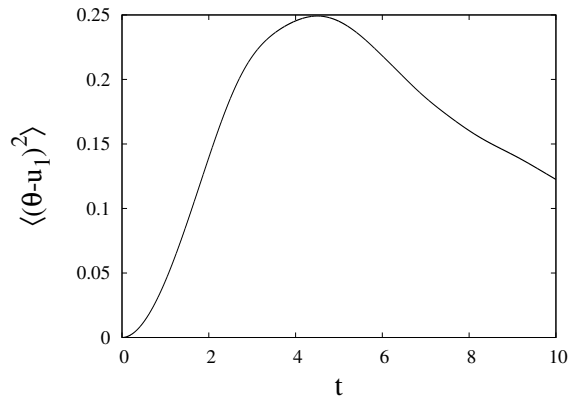


FIG. 10. Time evolution of $\langle (u_1 - \theta)^2 \rangle$ for the Navier-Stokes and passive scalar equations.

B. Performance of enstrophy bounds

Here we will consider the existing mathematical bounds for enstrophy growth. We will study their performance numerically, thereby quantifying the so-called depletion of nonlinearity. We define spatial integrals, which are *not* averaged by volume, as follows

$$E(t) = \frac{1}{2} \int |\mathbf{u}|^2 d\mathbf{x}, \quad Q(t) = \frac{1}{2} \int |\boldsymbol{\omega}|^2 d\mathbf{x} \quad \text{and} \quad P(t) = \frac{1}{2} \int |\nabla \times \boldsymbol{\omega}|^2 d\mathbf{x}. \quad (22)$$

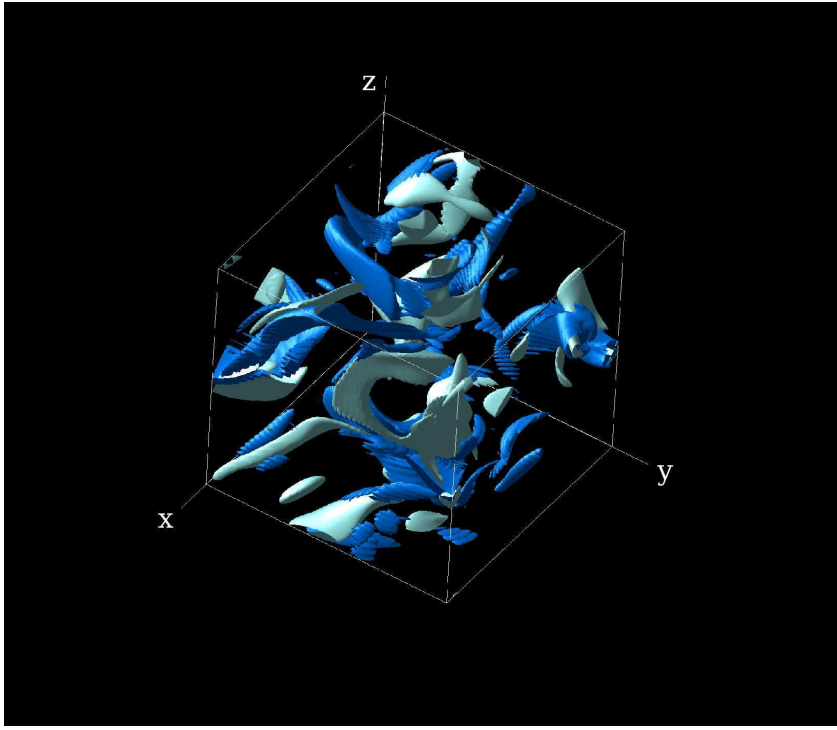


FIG. 11. Iso-surfaces of $|\boldsymbol{\omega}|^2$ (grey) and $(\theta - u_1)^2$ (white); $|\boldsymbol{\omega}|^2$ (blue) and $(\theta - u_1)^2$ (white) online, for the Navier-Stokes and passive scalar equations. The threshold is chosen as $|\boldsymbol{\omega}|^2 = 4 \langle |\boldsymbol{\omega}|^2 \rangle$ and $(\theta - u_1)^2 = 4 \langle (\theta - u_1)^2 \rangle$.

They correspond to squared L_2, H_1 and H_2 norms of the velocity, respectively.

It follows from the vorticity equation

$$\frac{\partial \boldsymbol{\omega}}{\partial t} + (\mathbf{u} \cdot \nabla) \boldsymbol{\omega} = (\boldsymbol{\omega} \cdot \nabla) \mathbf{u} + \nu \Delta \boldsymbol{\omega} \quad (23)$$

that

$$\frac{dQ}{dt} = \int \boldsymbol{\omega} \cdot (\nabla \mathbf{u}) \cdot \boldsymbol{\omega} d\mathbf{x} - \nu \int |\nabla \times \boldsymbol{\omega}|^2 d\mathbf{x}. \quad (24)$$

By standard procedures we can derive an enstrophy bound

$$\frac{dQ}{dt} \leq cQ^{3/4}P^{3/4} - 2\nu P \quad (25)$$

$$\leq \frac{c}{4}\nu^{-3}Q^3 - \frac{5}{4}\nu \frac{Q^2}{E(0)}. \quad (26)$$

(In inequalities in this paper c denotes positive constants, which may be different from each other.) This is done in two steps: 1) applications of the Cauchy-Schwartz and Gagliardo-Nirenberg inequalities to get (25) and 2) that of the Hölder inequality to get (26). The details may be found in e.g. [3, 30] and here we recall step 2 only.

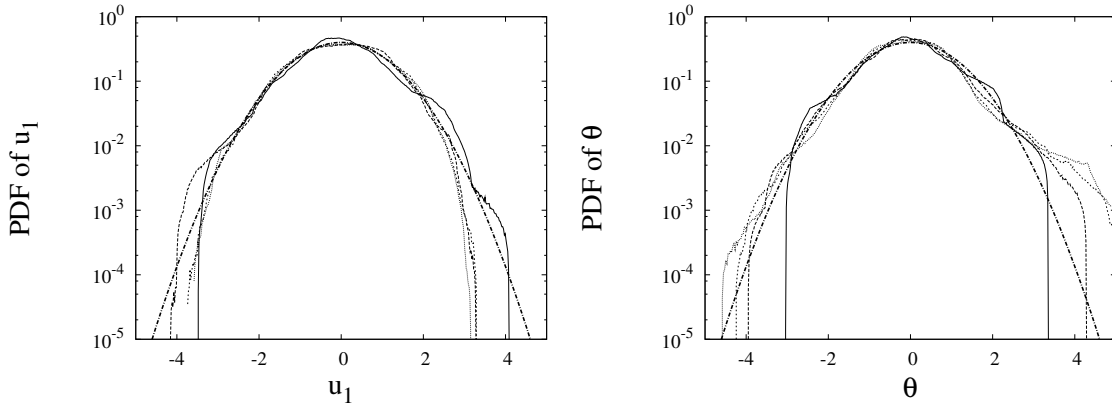


FIG. 12. PDFs of a) the velocity component u_1 of the Navier-Stokes equations (left) and b) passive scalar θ subject to the Navier-Stokes equations (right). Both are normalized to have unit variance: plotted at $t = 2$ (solid), 5 (dashed), 8 (short-dashed) and 10 (dotted). The thicker dot-dashed lines denote the standard normal distribution $N(0, 1)$.

We have $a^p b^q \leq pa + qb$ for $a, b > 0$ with $0 < p, q < 1, p + q = 1$ by a version of the Hölder inequality. Thus we find $cQ^{3/4}P^{3/4} = (c^4\nu^{-3}Q^3)^{1/4}(\nu P)^{3/4} \leq \frac{c^4}{4}\nu^{-3}Q^3 + \frac{3}{4}\nu P$. By the Cauchy-Schwartz inequality, we have $Q^2 \leq EP$ or $P \geq \frac{Q^2}{E} \geq \frac{Q^2}{E(0)}$. Renaming c^4 as c , we obtain (26). This procedure breaks down in four dimensional case $d = 4$ (see below) because we cannot take p or q to be equal to 1.

The well-known bound (26) has been discussed numerically in the literature, e.g. [30–34]. We note also that in the one-dimensional case we have

$$\frac{dQ}{dt} \leq c\nu^{-1/3}Q^{5/3} - 2\nu P, \quad (27)$$

which was studied in [24] and [30].

To study how the performance of mathematical estimates depend on the governing equations and the spatial dimensions they are defined in, we also consider the so-called quasi-4D (sometimes called 3.5D) Navier-Stokes equations. This class is defined by the following principle:

If \mathbf{u} solves the 3D Navier-Stokes equations, then by setting

$$\mathbf{u}_{4D} = \begin{pmatrix} \mathbf{u}(x_1, x_2, x_3, t) \\ \theta(x_1, x_2, x_3, t) \end{pmatrix}, \quad (28)$$

\mathbf{u}_{4D} solves the 4D Navier-Stokes equations because $\frac{\partial p}{\partial x_4} = 0$ [35]. It is a very special class of higher-dimensional Navier-Stokes flows, yet is physically relevant because the fourth component is a passive scalar. Care should be taken that genuine 4D Navier-Stokes flows cannot

be formed by this construction. With this reservation, it is still of interest what scaling behaviors the 3.5D Navier-Stokes flows exhibit. More general 4D Navier-Stokes equations have been discussed in a number of different contexts, see [36–43].

We note that Q has $[L^d T^{-2}]$ and ν has $[L^2 T^{-1}]$ as physical dimensions, where L, T denote length and time, respectively. We thus find on dimensional grounds in d -dimensions as a counterpart to (26),

$$\frac{dQ}{dt} \leq c\nu^{-\frac{d}{4-d}} Q(t)^{\frac{6-d}{4-d}}, \quad (29)$$

where we kept the contribution from nonlinear term only. Thus, as known in the folklore of mathematical fluid dynamics, at $d = 4$ the exponent $\frac{6-d}{4-d}$ becomes divergent and the bound becomes useless [44].

However, step 1 yields a bound in d -dimensions

$$\frac{dQ}{dt} + 2\nu P \leq cQ^{\frac{6-d}{4}} P^{\frac{d}{4}}, \quad (30)$$

which is still valid at $d = 4$. For the 4D Navier-Stokes equations, we have for the enstrophy bound

$$\frac{dQ}{dt} \leq cQ^{1/2} P - 2\nu P.$$

The mathematical results are summarized in the second column of Table II. We understand that in one dimension we redefine $E(t), Q(t)$ and $P(t)$, respectively by

$$E(t) = \frac{1}{2} \int u^2 dx, \quad Q(t) = \frac{1}{2} \int (\partial_x u)^2 dx, \quad \text{and} \quad P(t) = \frac{1}{2} \int (\partial_x^2 u)^2 dx. \quad (31)$$

Also, in four dimensions we replace $E(t)$ by $2\pi (E(t) + \frac{1}{2} \int |\theta|^2 \mathbf{d}\mathbf{x})$, $Q(t)$ by $2\pi (Q(t) + \frac{1}{2} \int |\nabla\theta|^2 \mathbf{d}\mathbf{x})$ and $P(t)$ by $2\pi (P(t) + \frac{1}{2} \int |\Delta\theta|^2 \mathbf{d}\mathbf{x})$, respectively. We examine performance of those bounds by numerical simulations.

We begin with the 1D Burgers equation under periodic boundary conditions

$$\frac{\partial u}{\partial t} + u \frac{\partial u}{\partial x} = \nu \frac{\partial^2 u}{\partial x^2} \quad (32)$$

with an initial condition

$$u(x, 0) = -\sin x \quad (33)$$

and viscosity $\nu = 5 \times 10^{-3}$. In view of

$$\frac{dQ}{dt} + 2\nu P \leq cQ^{5/4} P^{1/4}, \quad (34)$$

we plot in Fig.13 $\frac{dQ}{dt} + 2\nu P$ against $Q^{5/4}P^{1/4}$. Here we have estimated $\frac{dQ}{dt}$ by a finite-difference scheme in time. It shows a clear linear behavior with a slope close to 1 and also with a prefactor close to 1. In this sense, the inequality (34) is in fact very close to an *equality*, that is, it is doing a good job. (See Appendix C for a result with other initial data).

We show a similar plot in Fig.14 for the 3D Navier-Stokes equations. Unlike the 1D Burgers equation, no linear behavior is observed. In Fig.15 we try an alternative presentation, where $\frac{dQ}{dt} + 2\nu P$ is presented against $Q^{3/4}P^{3/4}$ in a log-log plot. It is noted that here we have a clear straight line behavior with a slope of about 0.4. In fact, the same scaling with the exponent is obtained even if we change the pseudo-random number sequences in the initial conditions (figures omitted). In the same figure, a corresponding plot is made for the quasi-4D Navier-Stokes equations as well. It also shows a power-law with exponent 0.4. These power-law behaviors imply that the bounds over-estimate the enstrophy growth excessively. Moreover, we can quantify the excess by determining the exponent, which may be regarded as a characterization of nonlinearity depletion. It is noted that the quasi-4D Navier-Stokes equations share the same exponent 0.4 with the 3D Navier-Stokes equations. One explanation for this is that the quasi-4D Navier-Stokes equations are essentially three-dimensional in character. We expect that if we do the same experiment using the genuine 4D Navier-Stokes equations they would show more depletion, with exponent < 0.7 .

In Fig.16 we compare the 3D Navier-Stokes with the 3D Burgers equations, using a similar log-log plot. The 3D Burgers equations show a similar power law behavior, but with an exponent 0.7 which is closer to 1 than that of 3D Navier-Stokes equations. This implies that while the bound over-estimates the enstrophy growth in 3D Burgers equations as well, the excess is not large in comparison with the 3D Navier-Stokes equations. In Fig.17, we put all the cases in one figure, where we can grasp the excesses of the mathematical bounds for different cases intuitively. Basically, as the graph is shifted to the right and the slope becomes shallower, the bounds over estimate the reality drastically.

Finally, we show a result of comparison of the 3D Navier-Stokes with Burgers equations

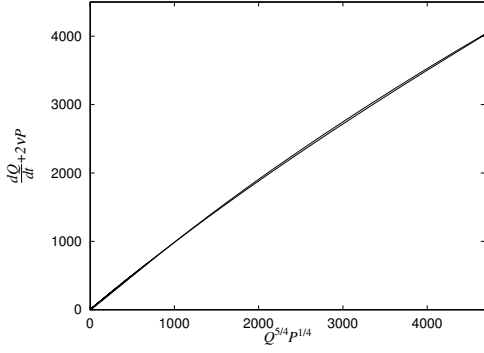


FIG. 13. Enstrophy growth for the 1D Burgers equation.

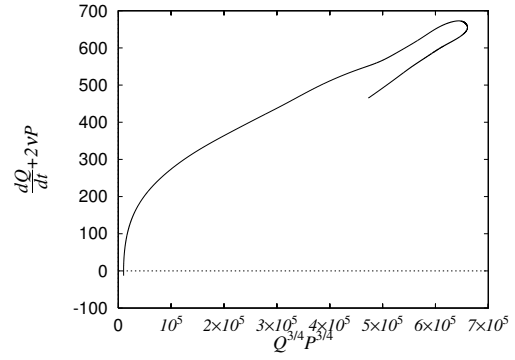


FIG. 14. Enstrophy growth for the 3D Navier-Stokes equations.

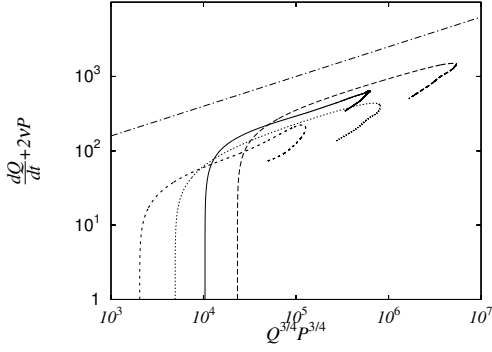


FIG. 15. Enstrophy growth for the 3D (solid) and quasi-4D (dashed) Navier-Stokes equations. The straight line denotes a slope 0.4. Also included are enstrophy growth for the 3D (dotted) and quasi-4D (short-dashed) for the Taylor-Green initial condition (see the subsequent discussion).

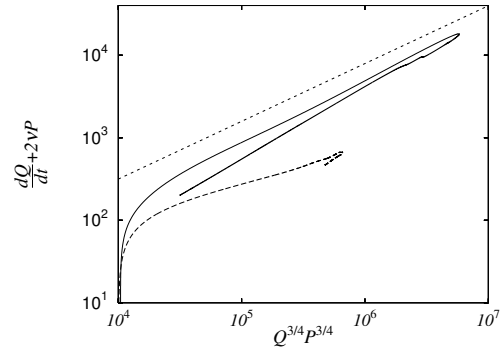


FIG. 16. Enstrophy growth for the 3D Burgers equations (solid) and the 3D Navier-Stokes equations (dashed). The straight line denotes a slope 0.7

using another initial condition (the Taylor-Green vortex). This is defined as follows

$$\begin{cases} u_1 = \cos x \sin y \sin z, \\ u_2 = -\sin x \cos y \sin z, \\ u_3 = 0. \end{cases} \quad (35)$$

In Fig.18 we compare energy norms. We see that the solenoidal component decays very quickly to zero. At late times, the entire flow field is dominated by the potential part. In terms of the enstrophy, the solenoidal part does not increase at all, but it monotonically

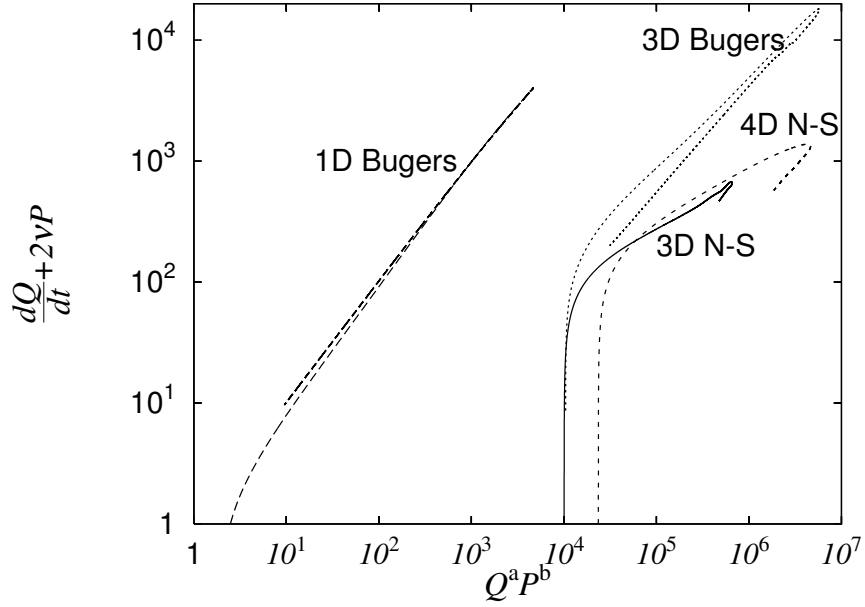


FIG. 17. Enstrophy growth for the 1D and 3D Burgers equations and for the 3D and quasi-4D Navier-Stokes equations.

TABLE II. Navier-Stokes and Burgers equations

equations	mathematical bounds	numerics	verdict
1D Burgers	$\frac{dQ}{dt} + 2\nu P \leq cQ^{5/4} P^{1/4}$	$\frac{dQ}{dt} + 2\nu P \approx Q^{5/4} P^{1/4}$	good
3D Navier-Stokes	$\frac{dQ}{dt} + 2\nu P \leq cQ^{3/4} P^{3/4}$	$\frac{dQ}{dt} + 2\nu P \propto (Q^{3/4} P^{3/4})^{0.4}$	over-estimate
3D Burgers	$\frac{dQ}{dt} + 2\nu P \leq cQ^{3/4} P^{3/4}$	$\frac{dQ}{dt} + 2\nu P \propto (Q^{3/4} P^{3/4})^{0.7}$	intermediate
quasi-4D Navier-Stokes	$\frac{dQ}{dt} + 2\nu P \leq cQ^{1/2} P$	$\frac{dQ}{dt} + 2\nu P \propto (Q^{1/2} P)^{0.4}$	over-estimate

decreases to zero (Fig.18). For the Navier-Stokes equations, the enstrophy attains its peak later and the peak value is lower than that of the Burgers equations. The dominance of the potential component is even more prominent in the case of Taylor-Green initial condition.

To conclude this section we comment on robustness of the power-laws found here. We have already mentioned that for different random initial conditions we observe the same power-laws. We point out that the power-law behavior (with $\alpha = 0.4$) is also observed for the Taylor-Green vortex, both with 3D and quasi-4D Navier-Stokes equations where we take $\theta = u_1$ initially, see Fig.15. Because it is a flow developing from a completely different initial condition, this indicates that such a power-law holds for a wider class of initial data. More work needs to be done to investigate how robust the scaling is.

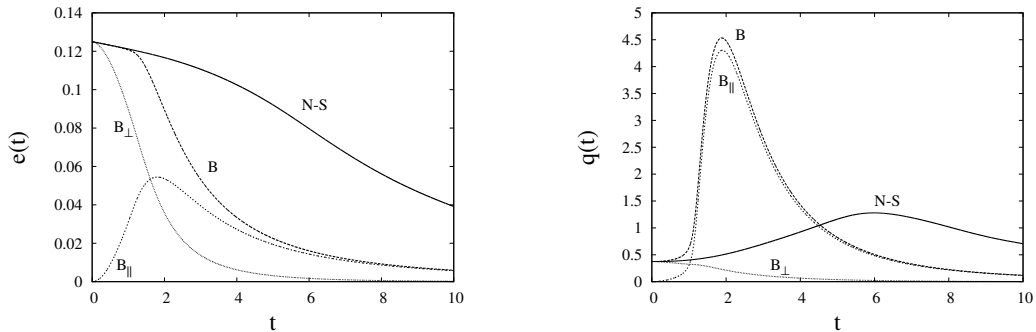


FIG. 18. Comparison of the norms for the Navier-Stokes and Burgers equations for the Taylor-Green vortex: (a) the energy (left) and (b) the enstrophy (right). Labels are as in Fig.1.

V. SUMMARY AND DISCUSSION

In this paper we have compared the Navier-Stokes equations with the Burgers equations and that of a passive scalar, centering on the effect of the absence or presence of the maximum principle.

In the PDF of the velocity, the Burgers equations have limited excitations at large amplitude, whereas the Navier-Stokes equations' wings are spread close to a Gaussian distribution. Breakdown of a maximum principle for the Navier-Stokes equations is due to the term $-\mathbf{u} \cdot \nabla p$ in the energy budget. Its PDF is basically symmetric, so are the joint PDFs of $-\mathbf{u} \cdot \nabla p$ with $\frac{1}{2}|\mathbf{u}|^2$ and $\frac{1}{2}|\boldsymbol{\omega}|^2$. This term neither contributes to enhance nor to avoid singularity formations, but simply makes the maximum principle invalid.

We have studied a passive scalar by initializing it as one component of the velocity, again to see the effect of the pressure term. Their deviation is maximized in the L^2 -norm, at a time between the peak times of the enstrophy and the average of the squared passive scalar gradient.

Finally, we have introduced a method for estimating performance of the enstrophy bounds (that is, a log-log plot at step 1) and tested it against numerical experiments. This includes the quasi-4D Navier-Stokes equations using the passive scalar as the fourth component. In contrast to the 1D Burgers equation, for the 3D Burgers equations the bound over-estimates the enstrophy growth to some degree. In the 3D and 4D Navier-Stokes equations, the excess is more significant. Thus the bounds are less sharp in higher dimensions and under the incompressible condition.

Let us consider an analogy. In [45] it was shown that if $\tilde{E}(k) \propto k^{-n}$, $n > \frac{8}{3}$ then the

energy spectral flux $\Pi(k) \rightarrow 0$ as $k \rightarrow \infty$ using flows with finite total kinetic energy. Here $\tilde{E}(k)$ denotes the energy spectrum based on the total energy. Indeed, if we use the total kinetic energy for dimensional analysis we would get [45]

$$\tilde{E}(k) \propto \tilde{\epsilon}^{2/3} k^{-8/3} \quad (36)$$

for the energy spectrum, where $\tilde{\epsilon}$ is the dissipation rate of total kinetic energy. Note that here $\tilde{E}(k)$ is an extensive variable, that is, it grows in proportion to its volume. This scaling is also consistent with global weak solutions of the Navier-Stokes equations, see [46].

Later, in connection with Onsager conjecture, a $r^{1/3}$ -behavior was derived in [47] using Besov space techniques (see also [48]). This of course is consistent with the Kolmogorov scaling

$$E(k) \propto \epsilon^{2/3} k^{-5/3}, \quad (37)$$

if we use energy and energy dissipation rate per unit volume, which are intensive variables themselves.

Standard mathematical analyses use extensive variables, such as the total enstrophy $Q(t)$ to find

$$\frac{dQ}{dt} \leq c \frac{Q^3}{\nu^3}, \quad (38)$$

However, if we use instead the enstrophy $q(t)$ per unit volume, we find

$$\frac{dq}{dt} \leq cq^{3/2} \quad (39)$$

in *any* spatial dimensions. Note that we may derive the above using the Karman-Howarth equation under the assumption of constancy of the skewness factor (see e.g. [33]). This suggests a possibility that using an intensive variable may improve the situation. Indeed, an envelope of volume averaged enstrophy follows (39), see [33]. Pursuing this line of analysis looks interesting, although it is yet to be justified.

ACKNOWLEDGMENTS

This work has been partially supported by an EPSRC grant EP/F009267/1 and by Royal Society. This work was presented as a poster at 'The Analysis of Incompressible Fluids, Turbulence and Mixing', in honor of Peter Constantin's 60th birthday, October 2011, Carnegie Mellon University. We are grateful to A. Biswas, P. Constantin, C. Foias and A. Larios for useful comments.

Appendix A: Cauchy formula for the Burgers equations

In the incompressible 3D Euler equations, vortex lines are material. In the 3D Burgers equations, vortex lines are still material but the first integrals should be modified. It is straightforward, but in view of the comparison of these two equations, it is best to state it here.

The vorticity equations read

$$\frac{\partial \boldsymbol{\omega}}{\partial t} + (\mathbf{u} \cdot \nabla) \boldsymbol{\omega} = (\boldsymbol{\omega} \cdot \nabla) \mathbf{u} - (\nabla \cdot \mathbf{u}) \boldsymbol{\omega}. \quad (\text{A1})$$

Introducing a new variable

$$\tilde{\boldsymbol{\omega}}(\mathbf{a}, t) = \boldsymbol{\omega}(\mathbf{a}, t) \exp \left(\int_0^t (\nabla \cdot \mathbf{u})(\mathbf{a}, t') dt' \right), \quad (\text{A2})$$

it satisfies

$$\frac{\partial \tilde{\boldsymbol{\omega}}}{\partial t} + (\mathbf{u} \cdot \nabla) \tilde{\boldsymbol{\omega}} = (\tilde{\boldsymbol{\omega}} \cdot \nabla) \mathbf{u}. \quad (\text{A3})$$

It follows from this

$$\tilde{\boldsymbol{\omega}}(\mathbf{a}, t) = \tilde{\boldsymbol{\omega}}(\mathbf{a}, 0) \cdot \frac{\partial}{\partial \mathbf{a}} \mathbf{x}(\mathbf{a}, t), \quad (\text{A4})$$

a generalized Cauchy formula. Because $\tilde{\boldsymbol{\omega}}$ -lines are frozen, so are $\boldsymbol{\omega}$ -lines. Noting that the Jacobian $J_{ij} = \frac{\partial x_i}{\partial a_j}$, ($i, j = 1, 2, 3$) satisfies

$$\frac{D\mathbf{J}}{Dt} = \mathbf{V}\mathbf{J}, \quad \mathbf{V} = \nabla \mathbf{u}, \quad (\text{A5})$$

where $\mathbf{x} = \mathbf{a}$ at $t = 0$. By Abel's formula

$$\frac{D}{Dt} \det \mathbf{J} = (\det \mathbf{J}) \text{tr} \left(\frac{D\mathbf{J}}{Dt} \mathbf{J}^{-1} \right), \quad (\text{A6})$$

we may write

$$\boldsymbol{\omega}(\mathbf{a}, t) = \frac{\mathbf{J}(\mathbf{a}, t) \cdot \boldsymbol{\omega}(\mathbf{a}, 0)}{|\det \mathbf{J}(\mathbf{a}, t)|} \quad (\text{A7})$$

or, equivalently

$$\boldsymbol{\omega}(\mathbf{a}, t) = \frac{\boldsymbol{\omega}(\mathbf{a}, 0) \cdot \frac{\partial}{\partial \mathbf{a}} \mathbf{x}(\mathbf{a}, t)}{\left| \det \left(\frac{\partial \mathbf{x}}{\partial \mathbf{a}} \right) \right|}. \quad (\text{A8})$$

Appendix B: Burgers gauge

We have seen that even if we take a general velocity field which has both solenoidal and potential parts, under the dynamics of the Burgers equations the potential part dominates quickly. We may ask whether and how we can find a field whose solenoidal part solves the Navier-Stokes equations whilst the potential part solves the Burgers equations. This is readily done by choosing an appropriate gauge in the so-called impulse formalism [49].

$$\frac{\partial \boldsymbol{\gamma}}{\partial t} = \mathbf{u} \times \boldsymbol{\omega} + \nabla \Lambda + \nu \Delta \boldsymbol{\gamma}, \quad (\text{B1})$$

$$\frac{\partial \phi}{\partial t} = p + \frac{|\mathbf{u}|^2}{2} + \Lambda + \nu \Delta \phi. \quad (\text{B2})$$

where the two scalar fields are related by $\lambda = \Lambda + \mathbf{u} \cdot \boldsymbol{\gamma}$. If we choose these as follows, “Burgers gauge”,

$$\Lambda = -p - \frac{|\mathbf{u}|^2 + |\nabla \phi|^2}{2}, \quad (\text{B3})$$

the potential part of $\boldsymbol{\gamma}$ solves the Burgers and the solenoidal part the Navier-Stokes equations.

Appendix C: Another initial condition for 1D Burgers equation

We test the bound (34) using another initial condition

$$u(x, 0) = -\sin x - \sin 2x. \quad (\text{C1})$$

As can be seen in Fig.19 Some deviation from (34) is noticeable at large amplitudes, while an overall scaling with $\alpha = 1$ works as an upper-bound.

-
- [1] C.R. Doering, “The 3D Navier-Stokes problem,” *Annu. Rev. Fluid Mech.* **41**, 1(2009).
 - [2] J.D. Gibbon, “Regularity and singularity in solutions of the three-dimensional Navier-Stokes equations,” *Proc. Roy. Soc. A* **466**, 2587(2010).
 - [3] C.R. Doering and J.D. Gibbon, *Applied Analysis of the Navier-Stokes Equations*, Cambridge, Cambridge University Press, 1995.
 - [4] P. Constantin, *Navier-Stokes equations*, Chicago, University of Chicago Press, 1988.

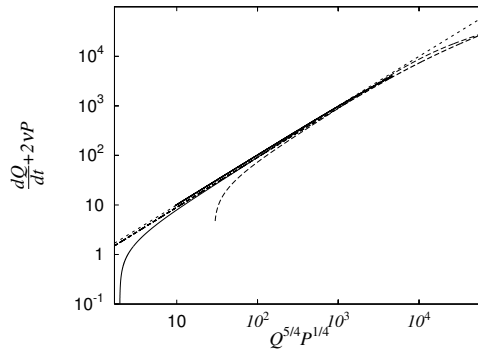


FIG. 19. Enstrophy growth for the 1D Burgers equation, the initial conditions (C1)(solid) and (33)(dashed). The dotted straight line denotes the bound (34) .

- [5] C. Foias, O. Manley, R. Rosa and R. Temam *Navier-Stokes Equations and Turbulence*, Cambridge, Cambridge University Press, 2001.
- [6] G. Gallavotti, “Some rigorous results about 3D Navier-Stokes,” Text of two lectures delivered at NATO-ASI meeting “Turbulence in spatially ordered systems”, Les Houches, 1992.
- [7] G. Gallavotti, *Foundations of Fluid Dynamics* (Springer, Berlin, 2002), Chap. 3, Sec. 3.5, pp. 209-212, pp. 212-214.
- [8] M. Arnold and W. Craig, “On the size of the Navier-Stokes singular set,” *Discret. Contin. Dyn. S.* **28**, 3 (2010).
- [9] A. Biryuk and W. Craig, “Bounds on Kolmogorov spectra for the Navier-Stokes equations,” *Commun. Pure Appl. Math.* **28**, 3 (2000).
- [10] T.Y. Hou, Z. Lei, “On the partial regularity of a 3D model of the Navier-Stokes equations,” *Commun. Math. Phys. Diff. Eq.* **287**, 2(2009).
- [11] C.L. Fefferman, *The Millennium Prize Problems* (American Mathematical Society, Providence, RI, 2006), pp. 57-70.
- [12] H.A. Rose and P.L. Sulem, “Fully developed turbulence and statistical mechanics,” *J. Phys. (Paris)* **39**, 5 (1978).
- [13] S.I. Chernyshenko, P. Constantin, J.C. Robinson and E.S. Titi, “A posteriori regularity of the three-dimensional Navier-Stokes equations from numerical computations,” *J. Math. Phys.* **48**, 6 (2007).

- [14] A. Pumir and E.D. Siggia, “Incipient singularities in the Navier-Stokes equations,” *Phys. Rev. Lett.* **55**, 17 (1987)
- [15] A. Pumir and E.D. Siggia, “Vortex dynamics and the existence of solutions to the Navier-Stokes equations,” *Phys. Fluids.* **30**, 5 (1987)
- [16] A. Pumir and E.D. Siggia, “Finite-time singularities in the axisymmetric three-dimension Euler equations,” *Phys. Rev. Lett.* **68**, 10 (1992)
- [17] K.R. Sreenivasan and C. Meneveau, “Singularities of the equations of fluid motion,” *Phys. Rev. E.* **38**, 12 (1988).
- [18] G. Rosen, “Navier-Stokes initial value problem for boundary-free incompressible fluid flow,” *Phys. Fluids* **12**, 2891 (1970).
- [19] J.G. Heywood, “Remarks on the possible global regularity of solutions of the three-dimensional Navier-Stokes equations,” *Pitman Res. notes Math. Ser.* **308**, 1 (1994).
- [20] A.A. Kiselev and O.A. Ladyzhenskaya, “On existence and uniqueness of the solutions of the nonstationary problem for a viscous incompressible fluid,” *Izv. Akad. Nauk SSSR Ser. Mat.* **21**, 655(1957), [*Am. Math. Soc. Transl. Ser.2*, **24**, 79(1957)].
- [21] C. Bardos, “Euler equation and burger equation - Relation with turbulence,” in *Nonlinear Partial Differential Equations and Applications*, *Lec. Notes in Math.* **648**, 1(1978).
- [22] C. Bardos, “Equations de Navier-Stokes et modèle de la turbulence,” *Journal de Physique* **39**, Colloques C5-53(1978).
- [23] C.V. Tran and D.G. Dritschel, “Energy dissipation and resolution of steep gradients in one-dimensional Burgers flows,” *Phys. Fluids* **22**, 037102(2010).
- [24] D. Ayala and B. Protas, “On Maximum Enstrophy Growth in a Hydrodynamics System,” *Physica D* **240**, 1553(2011).
- [25] K. Ohkitani, “A miscellany of basic issues on incompressible fluid equations,” *Nonlinearity.* **21**, 1 (2008).
- [26] F. Gesztesy and H. Holden, “The Cole-Hopf and Miura transformations revisited” in *Mathematical physics and stochastic analysis: essays in honour of Ludwig Streit*, p.198, (ed.) S. Albeverio, P. Blanchard, L. Ferreira, T. Hida, Y. Kondratiev, R. Vilela Mendes, World Scientific, 2000, Singapore.
- [27] T. Watanabe and T. Gotoh, “Statistics of a passive scalar in homogeneous turbulence,” *New Journal of Physics* **6**, 40(2004).

- [28] Consider an equation which is *linear* in θ ; $\frac{\partial\theta}{\partial t} + (\mathbf{u} \cdot \nabla)\theta = \nu\Delta\theta + f(\mathbf{x}, t)$ with a ‘forcing’ $f(\mathbf{x}, t) = -\frac{\partial p}{\partial x}$, where $\mathbf{u}(\mathbf{x}, t)$ and $p(\mathbf{x}, t)$ are taken from the Navier-Stokes solutions. By a uniqueness argument, if $\theta = u_1$ at $t = 0$, then $\theta = u_1$ for all $t > 0$ as long as \mathbf{u} remains smooth. If we drop ‘forcing’ we obtain (19).
- [29] B.B. Mandelbrot, “On the geometry of homogeneous turbulence, with stress on the fractal dimension of the iso-surfaces of scalars,” J. Fluid Mech. **72**, 3 (1975).
- [30] L. Lu and C.R. Doering, “Limits on enstrophy growth for solutions of the three-dimensional Navier-Stokes equations,” Indiana U. Math. J. **57**, 6 (2008).
- [31] P.E. Hamlington, J. Schumacher and W.J.A. Dahm, “Local and nonlocal strain rate fields and vorticity alignment in turbulent flows,” Phys. Rev. E. **77**, 11(2008).
- [32] P.E. Hamlington, J. Schumacher and W.J.A. Dahm, “Direct assessment of vorticity alignment with local and nonlocal strain rates in turbulent flows,” Phys. Fluids. **20**, 2(2008).
- [33] J. Schumacher, B. Eckhardt and C.R. Doering, “Extreme vorticity growth in Navier-Stokes turbulence,” Phys. Lett. A **374**, 861(2010).
- [34] P. Orlandi and S.P. Sergio, “Vorticity dynamics in turbulence growth,” Theor. Comput. Fluid Dyn. **24**, 247(2010).
- [35] R.J. DiPerna and A.J. Majda, “Oscillations and concentrations in weak solutions of the incompressible fluid equations,” Commun. Math. Phys. **108**, 667(1987).
- [36] T. Gotoh, Y. Watanabe, Y. Shiga, T. Nakano, E. Suzuki, “Statistical properties of four-dimensional turbulence,” Phys. Rev. E **75**, 016310(2007).
- [37] E Suzuki, T. Nakano, N. Takahashi and T. Gotoh, “Energy transfer and intermittency in four-dimensional turbulence,” Phys. Fluids, **17**, 081702(2005).
- [38] H. Dong and D. Du, “Partial Regularity of Solutions to the Four-Dimensional Navier-Stokes Equations at the First Blow-up Time,” Commun. Math. Phys. **273**, 785(2007).
- [39] T. Miyazaki, W. Kubo, Y. Shiga, T. Nakano and T. Gotoh, “Classical and quantum turbulence,” Physica D. **239**, 14(2010).
- [40] V. Scheffer, “The Navier-Stokes equations in space dimension four,” Commun. Math. Phys. **61**, 41(1978).
- [41] C. Gerhardt, “Stationary solutions to the Navier-Stokes equations in dimension four,” Math. Z. **165**, 193(1979).

[42] H. Kim, “Existence and Regularity of Very Weak Solutions of the Stationary Navier-Stokes Equations,” Arch. Rat. Mech. Anal. **193**, 117(2009).

[43] H. Liu, E. Tadmor and D. Wei, “Global Regularity of the 4D Restricted Euler Equations,” Phys. D **239**, 1225(2010).

[44] The reason for this is that at $d = 4$ the Gagliardo-Nirenberg inequality

$$\int |\boldsymbol{\omega}|^4 d\boldsymbol{x} \leq c \left(\int |\nabla \times \boldsymbol{\omega}|^2 d\boldsymbol{x} \right)^{d/2} \left(\int |\boldsymbol{\omega}|^2 d\boldsymbol{x} \right)^{2(1-d/4)}$$

reduces to the Sobolev lemma. Hence no application of the Hölder inequality is possible, because P would get an exponent 1.

[45] P.L. Sulem and U. Frisch, “Bounds on energy flux for finite energy turbulence,” J. Fluid Mech. **72**, 417(1975).

[46] C.R. Doering and J.D. Gibbon, “Bounds on moments of the energy spectrum for weak solutions of the three-dimensional Navier-Stokes equations,” Phys. D **165**, 163(2002).

[47] P. Constantin, W. E and E.S. Titi, “Onsager’s conjecture on the energy conservation for solutions of Euler’s equation,” Commun. Math. Phys. **165**, 207(1994).

[48] G.L. Eyink, “Energy dissipation without viscosity in ideal hydrodynamics I. Fourier analysis and local energy transfer,” Physica D: Nonlinear Phenomena, **78**, 222(1994).

[49] G. Russo and P. Smereka, Impulse formulation of the Euler equations: general properties and numerical methods,” J. Fluid Mech. **391**, 189(1991).